

The Fourth Catalog of Active Galactic Nuclei Detected by the *Fermi* Large Area Telescope - Data Release 3

M. AJELLO,¹ L. BALDINI,² J. BALLE³, D. BASTIERI,^{4,5,6} J. BECERRA GONZALEZ,⁷ R. BELLAZZINI,⁸ A. BERRETTA,⁹
E. BISSALDI,^{10,11} R. BONINO,^{12,13} A. BRILL,^{14,15} P. BRUEL,¹⁶ S. BUSON,¹⁷ R. CAPUTO,¹⁵ P. A. CARAVEO,¹⁸
C. C. CHEUNG,¹⁹ G. CHIARO,¹⁸ N. CIBRARIO,^{12,13} S. CIPRINI,^{20,21} M. CRNOGORCEVIC,^{22,15} S. CUTINI,²³ F. D'AMMANDO,²⁴
S. DE GAETANO,^{11,10} N. DI LALLA,²⁵ L. DI VENERE,^{10,11} A. DOMÍNGUEZ,²⁶ V. FALLAH RAMAZANI,²⁷
E. C. FERRARA,^{15,22,28} A. FIORI,² Y. FUKAZAWA,²⁹ S. FUNK,³⁰ P. FUSCO,^{10,11} V. GAMMALDI,³¹ F. GARGANO,¹¹
S. GARRAPPA,³² D. GASPARRINI,^{20,21} N. GIGLIETTO,^{10,11} F. GIORDANO,^{10,11} M. GIROLETTI,²⁴ D. GREEN,³³ I. A. GRENIER,³
S. GUIRIEC,^{34,15} D. HORAN,¹⁶ X. HOU,^{35,36} T. KAYANOKI,²⁹ M. KUSS,⁸ S. LARSSON,^{37,38} L. LATRONICO,¹² T. LEWIS,¹⁵
J. LI,^{39,40} I. LIODAKIS,⁴¹ F. LONGO,^{42,43} F. LOPARCO,^{10,11} B. LOTT,⁴⁴ M. N. LOVELLETTE,⁴⁵ P. LUBRANO,²³
G. M. MADEJSKI,²⁵ S. MALDERA,¹² A. MANFREDI,² G. MARTÍ-DEVESA,⁴⁶ M. N. MAZZIOTTA,¹¹ I. MEREU,^{9,23}
P. F. MICHELSON,²⁵ N. MIRABAL,^{15,47} W. MITTHUMSIRI,⁴⁸ T. MIZUNO,⁴⁹ M. E. MONZANI,^{25,50} A. MORSELLI,²⁰
I. V. MOSKALENKO,²⁵ M. NEGRO,^{28,47} R. OJHA,¹⁵ M. ORIENTI,²⁴ E. ORLANDO,^{51,25} J. F. ORMES,⁵² Z. PEI,⁵
H. PEÑA-HERAZO,^{13,53,12,54,55} M. PERSIC,^{43,56} M. PESCE-ROLLINS,⁸ V. PETROSIAN,²⁵ R. PILLERA,^{10,11} H. POON,²⁹
T. A. PORTER,²⁵ G. PRINCIPE,^{42,43,24} S. RAINÒ,^{10,11} R. RANDO,^{5,4,6} B. RANI,^{57,15,58} M. RAZZANO,² S. RAZZAQUE,⁵⁹
A. REIMER,⁴⁶ O. REIMER,⁴⁶ L. SCOTTON,⁶⁰ D. SERINI,¹¹ C. SGRÒ,⁸ E. J. SISKIND,⁶¹ G. SPANDRE,⁸ P. SPINELLI,^{10,11}
D. J. SUSON,⁶² H. TAJIMA,^{63,25} D. F. TORRES,^{64,65} J. VALVERDE,^{47,15} H. YASSIN,⁶⁶ AND G. ZAHARIJAS⁶⁷

¹Department of Physics and Astronomy, Clemson University, Kinard Lab of Physics, Clemson, SC 29634-0978, USA

²Università di Pisa and Istituto Nazionale di Fisica Nucleare, Sezione di Pisa I-56127 Pisa, Italy

³AIM, CEA, CNRS, Université Paris-Saclay, Université de Paris, F-91191 Gif-sur-Yvette, France

⁴Istituto Nazionale di Fisica Nucleare, Sezione di Padova, I-35131 Padova, Italy

⁵Dipartimento di Fisica e Astronomia "G. Galilei", Università di Padova, Via F. Marzolo, 8, I-35131 Padova, Italy

⁶Center for Space Studies and Activities "G. Colombo", University of Padova, Via Venezia 15, I-35131 Padova, Italy

⁷Instituto de Astrofísica de Canarias, Observatorio del Teide, C/Via Lactea, s/n, E-38205 La Laguna, Tenerife, Spain

⁸Istituto Nazionale di Fisica Nucleare, Sezione di Pisa, I-56127 Pisa, Italy

⁹Dipartimento di Fisica, Università degli Studi di Perugia, I-06123 Perugia, Italy

¹⁰Dipartimento di Fisica "M. Merlin" dell'Università e del Politecnico di Bari, via Amendola 173, I-70126 Bari, Italy

¹¹Istituto Nazionale di Fisica Nucleare, Sezione di Bari, I-70126 Bari, Italy

¹²Istituto Nazionale di Fisica Nucleare, Sezione di Torino, I-10125 Torino, Italy

¹³Dipartimento di Fisica, Università degli Studi di Torino, I-10125 Torino, Italy

¹⁴NASA Postdoctoral Program Fellow, USA

¹⁵NASA Goddard Space Flight Center, Greenbelt, MD 20771, USA

¹⁶Laboratoire Leprince-Ringuet, École polytechnique, CNRS/IN2P3, F-91128 Palaiseau, France

¹⁷Institut für Theoretische Physik and Astrophysik, Universität Würzburg, D-97074 Würzburg, Germany

¹⁸INAF-Istituto di Astrofisica Spaziale e Fisica Cosmica Milano, via E. Bassini 15, I-20133 Milano, Italy

¹⁹Space Science Division, Naval Research Laboratory, Washington, DC 20375-5352, USA

²⁰Istituto Nazionale di Fisica Nucleare, Sezione di Roma "Tor Vergata", I-00133 Roma, Italy

²¹Space Science Data Center - Agenzia Spaziale Italiana, Via del Politecnico, snc, I-00133, Roma, Italy

²²Department of Astronomy, University of Maryland, College Park, MD 20742, USA

²³Istituto Nazionale di Fisica Nucleare, Sezione di Perugia, I-06123 Perugia, Italy

²⁴INAF Istituto di Radioastronomia, I-40129 Bologna, Italy

²⁵W. W. Hansen Experimental Physics Laboratory, Kavli Institute for Particle Astrophysics and Cosmology, Department of Physics and SLAC National Accelerator Laboratory, Stanford University, Stanford, CA 94305, USA

²⁶Grupo de Altas Energías, Universidad Complutense de Madrid, E-28040 Madrid, Spain

²⁷Ruhr University Bochum, Faculty of Physics and Astronomy, Astronomical Institute (AIRUB), 44780 Bochum, Germany

²⁸Center for Research and Exploration in Space Science and Technology (CRESTT) and NASA Goddard Space Flight Center, Greenbelt, MD 20771, USA

²⁹Department of Physical Sciences, Hiroshima University, Higashi-Hiroshima, Hiroshima 739-8526, Japan

stefano.ciprini.asdc@gmail.com

dario.gasparrini@ssdc.asi.it

lott@cenbg.in2p3.fr

- ³⁰ *Friedrich-Alexander Universität Erlangen-Nürnberg, Erlangen Centre for Astroparticle Physics, Erwin-Rommel-Str. 1, 91058 Erlangen, Germany*
- ³¹ *Departamento de Física Teórica, Universidad Autónoma de Madrid, 28049 Madrid, Spain*
- ³² *Deutsches Elektronen Synchrotron DESY, D-15738 Zeuthen, Germany*
- ³³ *Max-Planck-Institut für Physik, D-80805 München, Germany*
- ³⁴ *The George Washington University, Department of Physics, 725 21st St, NW, Washington, DC 20052, USA*
- ³⁵ *Yunnan Observatories, Chinese Academy of Sciences, 396 Yangfangwang, Guandu District, Kunming 650216, P. R. China*
- ³⁶ *Key Laboratory for the Structure and Evolution of Celestial Objects, Chinese Academy of Sciences, 396 Yangfangwang, Guandu District, Kunming 650216, P. R. China*
- ³⁷ *Department of Physics, KTH Royal Institute of Technology, AlbaNova, SE-106 91 Stockholm, Sweden*
- ³⁸ *The Oskar Klein Centre for Cosmoparticle Physics, AlbaNova, SE-106 91 Stockholm, Sweden*
- ³⁹ *CAS Key Laboratory for Research in Galaxies and Cosmology, Department of Astronomy, University of Science and Technology of China, Hefei 230026, People's Republic of China*
- ⁴⁰ *School of Astronomy and Space Science, University of Science and Technology of China, Hefei 230026, People's Republic of China*
- ⁴¹ *Finnish Centre for Astronomy with ESO (FINCA), University of Turku, FI-21500 Piikkiö, Finland*
- ⁴² *Dipartimento di Fisica, Università di Trieste, I-34127 Trieste, Italy*
- ⁴³ *Istituto Nazionale di Fisica Nucleare, Sezione di Trieste, I-34127 Trieste, Italy*
- ⁴⁴ *Université Bordeaux, CNRS, LP2I Bordeaux, UMR 5797, F-33170 Gradignan, France*
- ⁴⁵ *The Aerospace Corporation, 14745 Lee Rd, Chantilly, VA 20151, USA*
- ⁴⁶ *Institut für Astro- und Teilchenphysik, Leopold-Franzens-Universität Innsbruck, A-6020 Innsbruck, Austria*
- ⁴⁷ *Department of Physics and Center for Space Sciences and Technology, University of Maryland Baltimore County, Baltimore, MD 21250, USA*
- ⁴⁸ *Department of Physics, Faculty of Science, Mahidol University, Bangkok 10400, Thailand*
- ⁴⁹ *Hiroshima Astrophysical Science Center, Hiroshima University, Higashi-Hiroshima, Hiroshima 739-8526, Japan*
- ⁵⁰ *Vatican Observatory, Castel Gandolfo, V-00120, Vatican City State*
- ⁵¹ *Istituto Nazionale di Fisica Nucleare, Sezione di Trieste, and Università di Trieste, I-34127 Trieste, Italy*
- ⁵² *Department of Physics and Astronomy, University of Denver, Denver, CO 80208, USA*
- ⁵³ *Instituto Nacional de Astrofísica, Óptica y Electrónica, Tonantzintla, Puebla 72840, Mexico*
- ⁵⁴ *Istituto Nazionale di Astrofisica-Osservatorio Astrofisico di Torino, via Osservatorio 20, I-10025 Pino Torinese, Italy*
- ⁵⁵ *East Asian Observatory, Hilo, HI 96720, USA*
- ⁵⁶ *Osservatorio Astronomico di Trieste, Istituto Nazionale di Astrofisica, I-34143 Trieste, Italy*
- ⁵⁷ *Korea Astronomy and Space Science Institute, 776 Daedeokdae-ro, Yuseong-gu, Daejeon 30455, Korea*
- ⁵⁸ *Department of Physics, American University, Washington, DC 20016, USA*
- ⁵⁹ *Centre for Astro-Particle Physics (CAPP) and Department of Physics, University of Johannesburg, PO Box 524, Auckland Park 2006, South Africa*
- ⁶⁰ *Laboratoire Univers et Particules de Montpellier, Université Montpellier, CNRS/IN2P3, F-34095 Montpellier, France*
- ⁶¹ *NYCB Real-Time Computing Inc., Lattingtown, NY 11560-1025, USA*
- ⁶² *Purdue University Northwest, Hammond, IN 46323, USA*
- ⁶³ *Solar-Terrestrial Environment Laboratory, Nagoya University, Nagoya 464-8601, Japan*
- ⁶⁴ *Institute of Space Sciences (ICE, CSIC), Campus UAB, Carrer de Magrans s/n, E-08193 Barcelona, Spain; and Institut d'Estudis Espacials de Catalunya (IEEC), E-08034 Barcelona, Spain*
- ⁶⁵ *Institució Catalana de Recerca i Estudis Avançats (ICREA), E-08010 Barcelona, Spain*
- ⁶⁶ *Centre for Space Research, North-West University, Potchefstroom Campus, Private Bag X6001, Potchefstroom 2520, South Africa*
- ⁶⁷ *Center for Astrophysics and Cosmology, University of Nova Gorica, Nova Gorica, Slovenia*

ABSTRACT

An incremental version of the fourth catalog of active galactic nuclei (AGNs) detected by the *Fermi*-Large Area Telescope is presented. This version (4LAC-DR3) derives from the third data release of the 4FGL catalog based on 12 years of $E > 50$ MeV gamma-ray data, where the spectral parameters, spectral energy distributions (SEDs), yearly light curves, and associations have been updated for all sources. The new reported AGNs include 587 blazar candidates and four radio galaxies. We describe the properties of the new sample and outline changes affecting the previously published one. We also introduce two new parameters in this release, namely the peak energy of the SED high-energy component and the corresponding flux. These parameters allow an assessment of the Compton dominance, the ratio of the Inverse-Compton to the synchrotron peak luminosities, without relying on X-ray data.

103
 104 *Keywords:* gamma rays: galaxies — gamma rays: observations — galaxies: active — galaxies: jets —
 105 BL Lacertae objects: general — quasars: general

106 1. INTRODUCTION

107 Since its launch in 2008, the *Fermi*-Large Area Telescope (LAT, Atwood et al. 2009) has enabled the discovery
 108 of new classes of gamma-ray emitters and the detection of much larger and better characterized source populations
 109 than previously achieved. Active galactic nuclei represent by far the most abundant source population of the LAT
 110 detected sources. The 4LAC catalog (4LAC-DR1, Ajello et al. 2020), based on the 4FGL source catalog (4FGL-DR1,
 111 Abdollahi et al. 2020) established with 8 years of data, comprised 2863 $|b| > 10^\circ$ AGNs while 344 others were found
 112 at lower latitudes. As more data accumulate, the catalogs are regularly updated. Updates of 4FGL use the same data
 113 version (“P8R3”) and Galactic diffuse emission model as the initial catalog. Sources previously reported are kept in
 114 even if they fall below the TS=25 threshold over the extended period of data taking. These sources retain their original
 115 positions, in contrast to new catalogs where all positions are reevaluated and subthreshold sources are omitted. The
 116 second data releases, 4FGL-DR2 (Ballet et al. 2020) and 4LAC-DR2 (comprising 285 new AGNs, Lott et al. 2020),
 117 were based on 10 years of data.

118 Here we present the third update to the 4LAC catalog, derived from 4FGL-DR3 (Abdollahi et al. 2022) using 12
 119 years of data and comprising 1607 new sources relative to the initial 4FGL catalog. The properties of the 283 new
 120 4FGL-DR2¹ and 308 new 4FGL-DR3 AGNs (DR2 and DR3 tallies will be aggregated in the following) are discussed.
 121 These AGNs are all blazars except for four radio galaxies. Besides providing a larger AGN sample for population
 122 studies, releasing periodic updates to 4LAC offers new targets for programs dedicated to classifying LAT blazars or
 123 measuring redshifts as detections come along (e.g., Peña-Herazo et al. 2020, 2021a,b,c; Desai et al. 2019; Rajagopal
 124 et al. 2021; Goldoni et al. 2021).

125 The paper is organized as follows. Section 2 summarizes the analysis improvements introduced in 4FGL-DR3.
 126 Changes affecting 4LAC-DR1 AGNs are listed in Section 3. Section 4 presents the new DR3 sources, while Section 5
 127 discusses the peak energy of the SED high-energy component, estimated from the spectral curvature, and the derived
 128 Compton dominance. A summary closes the paper in Section 6.

129 2. ANALYSIS IMPROVEMENTS - SOURCE ASSOCIATIONS

130 We refer the reader to the 4FGL-DR3 paper (Abdollahi et al. 2022) for details on the gamma-ray data analysis. The
 131 methodology that was followed is essentially the same as that pursued in the 4FGL-DR1 catalog. The first stage includes
 132 the detection and localization of the sources. The second one comprises thresholding, spectral characterization and
 133 production of light curves. The same flags as in 4FGL-DR1 are then generated. They indicate the limited robustness
 134 of the results against different analysis ingredients or warning about particular source conditions (e.g., proximity to
 135 a bright source). The association with counterparts known at other wavelengths constitutes the final stage of the
 136 analysis.

137 The (non-exhaustive) list of changes relative to 4FGL-DR1² is as follows. An updated version of the instrument-
 138 response functions (P8R3_SOURCE_V3) has been used. The analysis weights have been recalculated. These weights
 139 downplay the contribution of low-energy, low-latitude photons to the likelihood in order to reduce the associated
 140 systematic uncertainties. The handling of the energy dispersion has been improved. Bayesian priors have been applied
 141 when fitting the parameters of the diffuse emission model in each region of interest to hinder their excursion relative to
 142 their expected values (normalization =1, photon-index correction=0). The threshold for considering spectral curvature
 143 as significant has been lowered from 3σ to 2σ , leading to an increase of the fraction of curved sources from 30% in
 144 4FGL-DR1 to 54% in 4FGL-DR3. This change has removed unphysical upturns in the global source spectrum at
 145 low (< 200 MeV) and high (> 20 GeV) energy. It has important implications for the characterization of the LAT
 146 blazars since the peak energy of the SED high-energy component (referred to as the Inverse-Compton component in
 147 the following, assuming that relativistic electrons are the main emitting particles) and its flux can be derived from

¹ Two AGNs first reported in DR2 are missing in DR3 because the gamma-ray sources (4FGL J1242.4–2948 and 4FGL J1752.2–3002) have been either relocalised or deleted (being exceptions to the rule stated above).

² DR2 was produced with only minor analysis changes relative to DR1.

the fitted logparabola. The number of bins in the SED has been increased from 7 to 8. The yearly light curves have been updated (while the two-monthly ones reported in 4FGL-DR1 have not). Specific to the 4LAC update, the highest photon energy detected for each source has been updated. The information about the highest detected energy is particularly relevant for studies of the extragalactic background light (EBL, e.g., [Saldana-Lopez et al. 2021](#)).

The association procedure makes use of two different methods, the Bayesian method ([Abdo et al. 2010b](#)) and the likelihood-ratio method (LR, [Ackermann et al. 2011, 2015](#)), which are both based on spatial coincidence. The main change in seeking counterparts concerns the use of an updated version of the Radio Fundamental Catalog³. Only associations with a probability of being real greater than 0.8 in either association method are retained. For the 591 new AGNs, 253 are associated solely with the Bayesian method, 65 solely with the LR method and 273 with both methods.

The same classification scheme as in the 4LAC-DR1 catalog has been followed. An optical class in terms of Flat Spectrum Radio Quasar (FSRQ) and BL Lac-type object (BL Lac), assessed according to the strength of the optical emission lines, is provided if spectroscopic data of sufficiently good quality are found in the literature. A SED-based class is derived from the value of the peak frequency ($\nu_{\text{pk}}^{\text{syn}}$) of the synchrotron component fitted to archival data using the SED data archive and SED(t)-Builder interactive web-tool available at the Italian Space Agency (ASI) Space Science Data Center (SSDC)⁴. The class can be a low-synchrotron-peaked blazar (LSP, for sources with $\nu_{\text{pk}}^{\text{syn}} < 10^{14}$ Hz), an intermediate-synchrotron-peaked blazar (ISP, for 10^{14} Hz $< \nu_{\text{pk}}^{\text{syn}} < 10^{15}$ Hz), or a high-synchrotron-peaked blazar (HSP, if $\nu_{\text{pk}}^{\text{syn}} > 10^{15}$ Hz). SED-based classification is missing for 139 new AGNs, mainly because of a lack of broad-band data.

3. CHANGES TO 4LAC-DR1

For completeness, we reiterate here the changes to 4LAC-DR1 AGNs as outlined in the 4FGL-DR2 document ([Lott et al. 2020](#)). About 200 counterpart names of DR1 sources have been changed. It was noted that blazar names from very large surveys (such as 2MASS or WISE) were used for some 4FGL associations while more common names from radio catalogs were available. Moreover some names referred to sources that are offset by up to a few arcminutes from the real counterpart. We have replaced the non-radio names with those of radio counterparts whenever possible. Note that the positions reported in the 4FGL-DR1 (RA_Counterpart, DEC_Counterpart) fields were correct.

Changes in associations of 4LAC-DR1 sources are listed below.

- Recent follow-up observations of 4FGL blazars (e.g., [Peña-Herazo et al. 2017, 2019, 2020, 2021a,b,c](#); [Desai et al. 2019](#); [Rajagopal et al. 2021](#)) have enabled the classification of 240 former blazar candidates of unknown types (BCUs), two AGNs and two UNKs⁵ into 214 BL Lacs and 30 FSRQs. In particular, [Paliya et al. \(2020a\)](#) found that the former BCU associated with 4FGL J1219.0+3653 is a BL Lac with a redshift of 3.53, making it the most distant BL Lac detected by the LAT.
- The latest version of the Radio Fundamental Catalog has enabled the association with blazar candidates of six previously unassociated sources and two SPPs (SPPs designate potential associations with supernova remnants or pulsar-wind nebulae). These sources are 4FGL J0129.0+6312 (2MASS J01283059+6306298), 4FGL J0550.9+2552 (NVSS J055119+254909), 4FGL J0803.5+2046 (GB6 B0800+2046), 4FGL J1102.0−6054 (2MASS J11015838−6056516), 4FGL J1347.4+7309 (NVSS J134734+731812), 4FGL J1606.6+1324 (NVSS J160654+131934), 4FGL J1738.0+0236 (PKS 1735+026), and 4FGL J2249.9+0452 (WISEA J225007.35+045617.3).
- Three sources (TXS 0159+085, PKS 0736−770, and TXS 1530−131) were incorrectly classified as FSRQs. They have been reclassified as BCUs. Two other FSRQs (RX J0134.4+2638 and 2MASS J02212698+2514338) have been reclassified as BL Lacs⁶.
- Following [Järvelä et al. \(2020\)](#), we have reclassified TXS 2116−077 (4FGL J2118.8−0723) as a Seyfert galaxy instead of a NLSY1 (see [Paliya et al. 2020b](#), for an alternative view).

³ rfc_2021a available at <http://astrogeo.org/rfc/>

⁴ <http://tools.ssdsc.asi.it/SED/>

⁵ The UNK class corresponds to $|b| < 10^\circ$ sources solely associated with the LR-method, which may suffer from contamination with Galactic sources.

⁶ TXS 0159+085 and RX J0134.4+2638 were still classified as FSRQs in 4FGL-DR3.

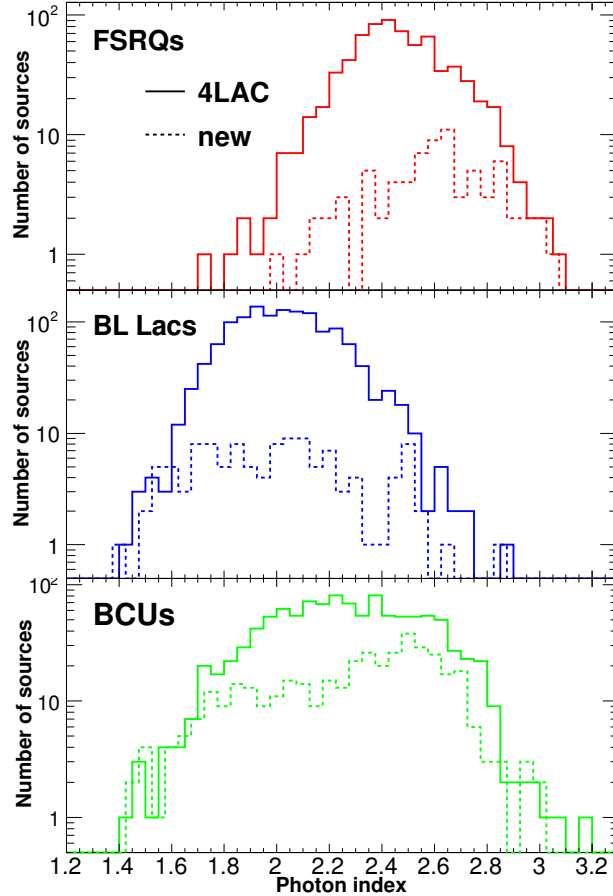


Figure 1. Comparison between the photon index distributions of 4LAC-DR1 and new (DR2 and DR3) blazars for different classes.

- The tentative association of 4FGL J0647.7–4418 with the high-mass X-ray binary RX J0648.0–4418 reported in 4FGL-DR1 has been replaced by the association with the BCU SUMSS J064744–441946 following the multi-wavelength investigation of Martí et al. (2020).

A total of 214 additional 4LAC-DR1 sources are now classified as variable thanks to the extended yearly light curves produced in DR3. These sources comprise 26 FSRQs, 105 BL Lacs, 80 BCUs, and three radio galaxies (IC 1531, PKS 0625–35, and Cen A). Concerning the iconic radio galaxy Cen A, its flux dropped significantly (14%) in the last four years spanned by this release.

Photons with higher energies than previously detected in the earlier 8 years have been found for 471 4FGL-DR1 sources during the additional 4 years of data taking. Only $E > 10$ GeV, ULTRACLEAN_VETO photons with a probability greater than 0.95 to belong to the source have been considered.

4. THE 4LAC-DR3 AND LOW-LATITUDE SAMPLES

The 4LAC-DR3 sample comprises AGNs located at $|b| > 10^\circ$, in keeping with the 4LAC defining criterion. The same defining criterion for the clean sample (i.e., sources with no analysis flags) as in 4LAC-DR1 has been used in this paper. The AGNs lying at $|b| < 10^\circ$ constitute the low-latitude sample.⁷ Table A1 describes the format of the catalog FITS files.

The new AGNs relative to 4LAC-DR1 include 587 blazars: 75 FSRQs, 117 BL Lacs, 395 BCUs, and four radio galaxies (8 BCUs have been classified into 7 BL Lacs and one FSRQ since the DR2 release). The 4LAC-DR3 comprises 542

⁷ The 4LAC-DR3 and low-latitude files are available at <https://fermi.gsfc.nasa.gov/ssc/data/access/lat/4LACDR3/table-4LAC-DR3-h.fits> and <https://fermi.gsfc.nasa.gov/ssc/data/access/lat/4LACDR3/table-4LAC-DR3-l.fits> respectively.

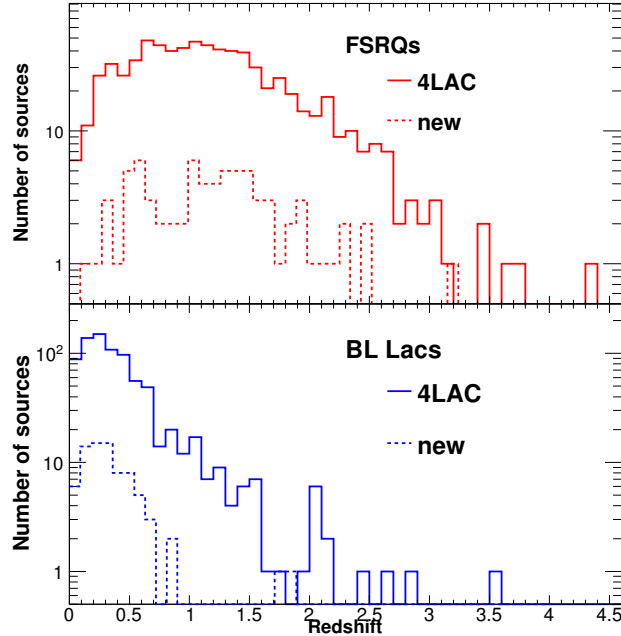


Figure 2. Comparison between the redshift distributions of 4LAC-DR1 and new (DR2 and DR3) blazars for different classes.

210 ($|b| > 10^\circ$) new AGNs. While FSRQs are almost evenly distributed between the northern and southern Galactic
 211 hemispheres (40 and 35 respectively), a strong deficit is observed in the South for BL Lacs (80 vs. 37), while the
 212 opposite trend is seen for BCUs (166 vs. 229). These imbalances are probably due to fewer programs observing the
 213 southern region. The low-latitude sample includes 49 sources (all BCUs except for one BL Lac).

214 Table 1 gives the census of the new AGNs, while Table 2 provides that of the whole population. Figures 1 and 2
 215 compare the photon-index and redshift distributions respectively between the new and 4LAC-DR1 samples for different
 216 blazar classes.

217 The median photon index of the new FSRQs is larger (2.61 vs 2.45) than that of the DR1 sample, indicating softer
 218 spectra. The median redshift is similar to 4LAC-DR1 (1.19 vs. 1.12). PKS 2318–087 (4FGL J2320.8–0823) with
 219 $z=3.164$ has the highest redshift of the new 4LAC-DR3 FSRQs, though four 4LAC-DR1 FSRQs have higher redshifts
 220 (up to 4.31). A total of 32 new FSRQs (7 of them with $TS > 100$) are found to be variable and 12 of them, which are
 221 more significant than average, show pronounced flares in the last 4 years of the 12-yr period.

222 Of the 117 new BL Lacs, a SED-based classification could be obtained for 94 of them, comprising 22 LSPs, 27 ISPs,
 223 46 HSPs. The new BL Lacs have a median photon index similar to the DR1 ones (2.00 vs. 2.03). The median redshift
 224 of the 78 BL Lacs with measured values is 0.28, which is comparable to that of 4LAC-DR1 (0.34). The maximum
 225 redshift is 0.848 for RX J1438.3+1204 (4FGL J1438.6+1205), while the maximum redshift of 4LAC-DR1 BL Lacs is
 226 3.53. Only 6 new BL Lacs (all with $TS < 100$) are found to be variable.

227 BCUs represent more than two thirds of the new blazars due to a lack of reliable spectroscopic data. Some insight
 228 into the nature of these sources can nevertheless be gained by inspecting their photon index distributions, building
 229 on the remarkably distinct distributions exhibited by FSRQs and BL Lacs. The BCU distribution, with a median
 230 photon index notably higher than the corresponding DR1 value (i.e., 2.36 and 2.23 respectively), is compared to the
 231 (normalized) FSRQ and BL Lac distributions in Figure 3. To best reproduce the BCU distribution with a linear
 232 combination of the latter distributions, the relative weight of FSRQs must be increased by a factor $\simeq 2.5$ with respect
 233 to that found in the 4LAC-DR3 sample. In 4LAC-DR1, the BCU distribution could be well reproduced by assuming
 234 the same fractions of FSRQs and BL Lacs as found in the classified population (see Figure 6 in Ajello et al. 2020).
 235 This excess of new FSRQ candidates in 4LAC-DR3 may come from the stronger flaring activity of FSRQs relative to

Table 1. Census of new DR2-DR3 sources

AGN type	High-latitude sample	Clean Sample ^a	Low-latitude sample
All	542	430	49
FSRQ	75	56	0
... LSP	67	49	0
... ISP	5	5	0
... HSP	1	1	0
... no SED classification	2	1	0
BL Lac	116	97	1
... LSP	22	20	1
... ISP	27	19	0
... HSP	46	40	0
... no SED classification	21	18	0
Blazar of Unknown Type	347	273	48
... LSP	172	130	26
... ISP	35	29	4
... HSP	41	38	1
... no SED classification	99	76	17
Non-blazar AGN	4	4	0
... RG	4	4	0

^aSources in the high-latitude sample without analysis flags.

236 BL Lacs in the LAT energy range. The photon-index distribution of the 77 variable BCUs, with 15 of them having
 237 TS>100, supports this idea (Figure 4). **The observation of slightly softer spectra relative to the bulk of**
 238 **FSRQs for both the new FSRQ-like BCUs and the new FSRQs is compatible with this explanation.**
 239 **This effect holds for sources of both classes with detected variability.** Out of the 396 new BCUs, only 7
 240 have measured redshifts. These have photon indices similar to those of FSRQs. This observation applies to the whole
 241 population of BCUs with measured redshifts.

242 The four new radio galaxies are NGC 3078, NGC 4261, LEDA 55267, and NGC 6454. NGC 3078 is a nearby (d=35
 243 Mpc) compact-core-dominated galaxy (Wrobel & Heeschen 1984). NGC 4261 (d=30 Mpc) is a LINER Fanaroff-Riley
 244 type-I (FR I) radio galaxy, whose LAT detection was first reported by de Menezes et al. (2020). The detection of
 245 LEDA 55267 was first reported by Paliya (2021). It was classified there as a Fanaroff-Riley type-0 radio galaxy, i.e.,
 246 having similar nuclear and host properties as FR I's but significantly fainter extended radio emission (Grandi et al.
 248 2016). NGC 6454 is a FRI galaxy (Britzen et al. 2008; van Velzen et al. 2012) at a distance of 130 Mpc⁸.

249 5. PEAK ENERGY OF THE HIGH-ENERGY COMPONENT - COMPTON DOMINANCE

250 Two new parameters are provided in the DR3 release for the whole set of LAT blazars: the peak energy ($E_{\text{pk}}^{\text{IC}}$),
 251 or equivalently the peak frequency ($\nu_{\text{pk}}^{\text{IC}}$), and the corresponding flux (νF_{ν}^{IC}) of the SED high-energy component in
 252 the observer frame. Thanks to the improved statistics and the relaxed threshold for considering spectral curvature as
 253 significant, 1601 LAT blazars have a significantly curved spectrum, from which these two parameters can be estimated
 254 using a fit of a log normal function. This assessment of $E_{\text{pk}}^{\text{IC}}$ is an alternative to that based on a polynomial fit to the
 255 IC component using both X-ray and gamma-ray data (e.g., as in Abdo et al. 2010a). The latter assessment may suffer
 256 from the fact that multiple processes can contribute to the IC component, making its actual shape uncertain. Here

⁸ This source was classified as an "AGN" in 4FGL-DR3.

Table 2. Census of 4LAC-DR3 sources

AGN type	High-latitude sample	Clean Sample ^a	Low-latitude sample
All	3407	2896	407
FSRQ	755	640	37
... LSP	672	581	35
... ISP	20	18	0
... HSP	4	4	0
... no SED classification	59	37	2
BL Lac	1379	1261	79
... LSP	353	332	20
... ISP	347	309	8
... HSP	425	394	29
... no SED classification	254	226	22
Blazar of Unknown Type	1208	945	285
... LSP	508	397	78
... ISP	135	115	12
... HSP	117	99	10
... no SED classification	448	334	185
Non-blazar AGN	65	50	6
... RG	42	32	4

^aSources in the high-latitude sample without analysis flags.

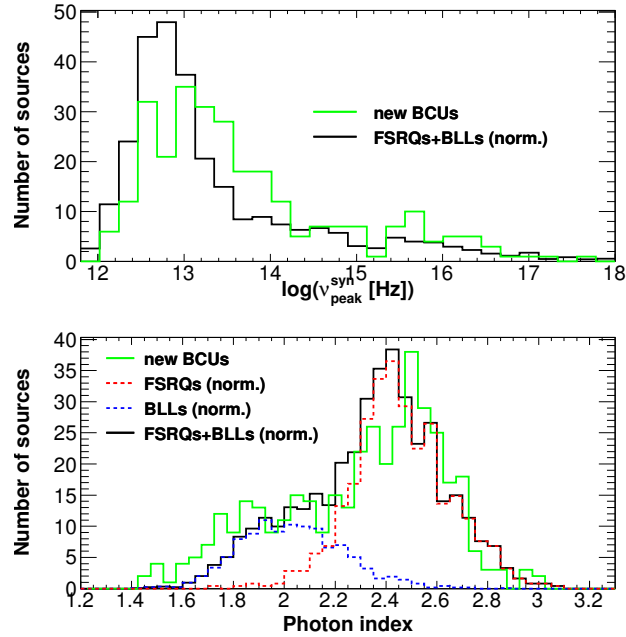


Figure 3. Distributions of $\nu_{\text{pk}}^{\text{syn}}$ (top) and photon index (bottom) of the new (DR2 and DR3) BCUs (green solid) compared to the arbitrarily normalized sum of the FSRQ and BL Lac distributions (solid black). The relative weight between FSRQs and BL Lacs has been multiplied by 2.5 with respect to that found in 4FGL.

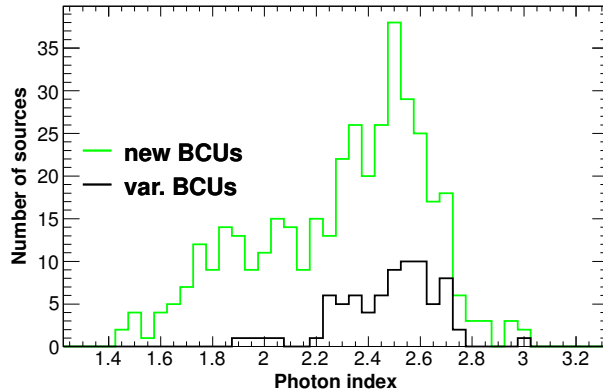


Figure 4. Photon index distributions for the new BCUs and the subset of sources showing significant variability.

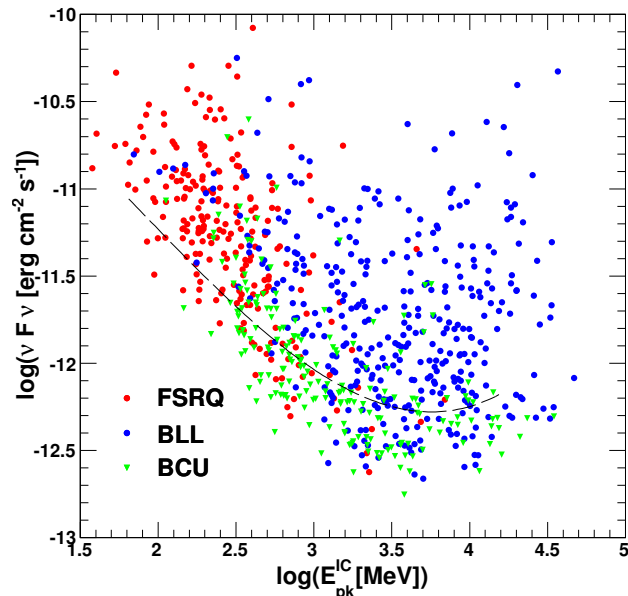


Figure 5. $\nu F\nu$ of the high-energy peak as a function of the peak energy for sources fulfilling the conditions given in the text. Error bars have been omitted for clarity. The dashed curve corresponds to an estimated average threshold.

257 we restrict the discussion to sources with a relative uncertainty on $E_{\text{pk}}^{\text{IC}}$ lower than 50%. This condition favors sources
 258 with slightly harder gamma-ray spectra than average. The effect is more pronounced for FSRQs (mean photon index
 259 difference relative to the whole sample, $\Delta\Gamma=0.08$), and diminishes for BL Lacs as $\nu_{\text{pk}}^{\text{syn}}$ increases (from $\Delta\Gamma=0.05$ for
 260 LSPs to $\Delta\Gamma=0.03$ for HSPs). Overall, the fraction of sources with $E_{\text{pk}}^{\text{IC}}$ meeting the above condition is 30%, 28% and
 261 24% for FSRQS, BL Lacs, and BCUs respectively. FSRQs preferentially exhibit $E_{\text{pk}}^{\text{IC}}$ below 1 GeV, while most BL Lacs
 262 have $E_{\text{pk}}^{\text{IC}}$ above this value, reflecting the dichotomy seen in the photon-index distributions (Figure 1). Most values
 263 of $E_{\text{pk}}^{\text{IC}}$ obtained for the 9 radio galaxies meeting the above condition are notably larger than those reported from a
 264 combined fit to the X-ray and gamma-ray data (see e.g., Fukazawa et al. 2022). An explanation for this discrepancy
 265 can be the presence of a prominent emission from the corona/accretion disk in the X-ray to soft gamma-ray bands,
 266 which drives down the fitted $E_{\text{pk}}^{\text{IC}}$ value in the latter case.

267 Except in very rare cases (5 sources), $E_{\text{pk}}^{\text{IC}}$ lies within the *Fermi*-LAT energy range ($E_{\text{pk}} > 50$ MeV) and is thus
 268 reasonably well constrained on the lower-energy side. In the following, we apply no corrections for the extinction due
 269 to the extragalactic background light, which affects $E > 10$ GeV photons. Reported values of $E_{\text{pk}}^{\text{IC}}$ greater than 10 GeV

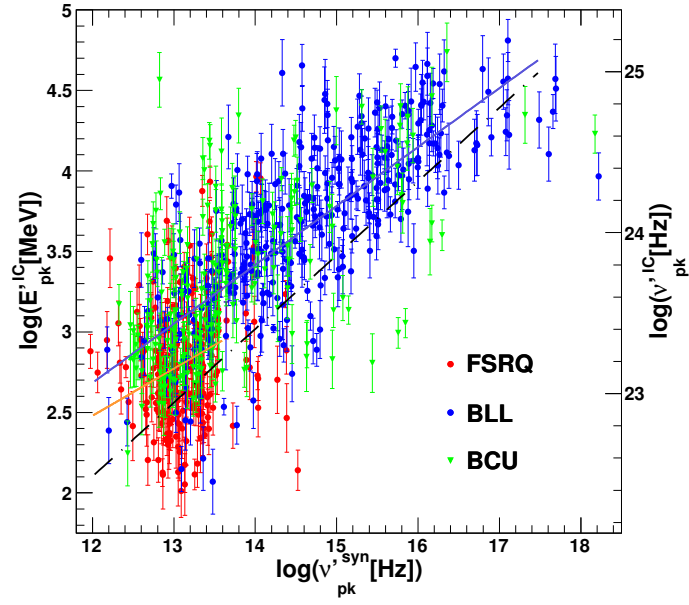


Figure 6. Energy of the high-energy component plotted as a function of $\nu'_{pk}{}^{\text{syn}}$, both estimated in the rest frame, for the different blazar classes. The source selection is described in the text. The blue line represents a linear fit to the BL Lac data and the orange one (restricted to $\log(\nu'_{pk}{}^{\text{syn}}) < 13.6$) to the FSRQ data. The black dash-dotted line corresponds to the prescription from Abdo et al. (2010a).

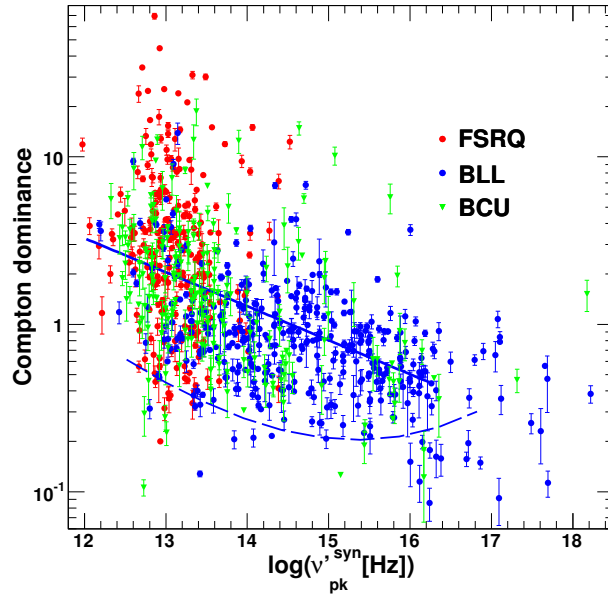


Figure 7. Compton dominance plotted as a function of $\nu'_{pk}{}^{\text{syn}}$ for the same sources as in Figure 6. The dashed line corresponds to an estimate of the average threshold for BL Lacs (derived from the threshold plotted in Figure 5) and the solid line to an exponential fit to the BL Lac data.

must thus be considered as lower limits, as must the associated νF_ν^{IC} values. Figure 5 displays νF_ν^{IC} as a function of $E_{\text{pk}}^{\text{IC}}$. An estimated threshold for determining the two parameters with the required significance/accuracy is plotted in this Figure. This threshold was calculated as a polynomial fit to the data of blazars with $\Delta E_{\text{pk}}^{\text{IC}} = (50 \pm 5)\%$.

A detailed study of blazar populations is beyond the scope of this paper so we just outline some broad features. The synchrotron peak frequency could be determined for 785 of these blazars, including 230 FSRQs, 362 BL Lacs, and 193 BCUs. In a simple single-zone synchrotron self-Compton (SSC) model and assuming Inverse-Compton scattering in the Thomson regime, the peak Lorentz factor of the electron distribution γ_{SSCpk} most contributing to the electromagnetic emission can be directly assessed in a redshift-independent way from the two peak frequencies $\gamma_{\text{pk}}^{\text{SSC}} = \left(\frac{3\nu_{\text{pk}}^{\text{IC}}}{4\nu_{\text{pk}}^{\text{syn}}}\right)^{1/2}$. These frequencies, evaluated in the source rest frame⁹, are plotted as a function of one another in Figure 6. We emphasize that the estimates of $\nu_{\text{pk}}^{\text{syn}}$ and $E_{\text{pk}}^{\text{IC}}$ are obtained independently, so near-empty regions in Figure 6 do not result from an observational or analysis bias. BCUs follow the same general trend seen for FSRQs and BL lacs.

The correlation between $\nu_{\text{pk}}^{\text{syn}}$ and $E_{\text{pk}}^{\text{IC}}$ is strong for BL Lacs (Pearson coefficient=0.75) but weak for FSRQs (Pearson coefficient=0.08 for $\log(\nu_{\text{pk}}^{\text{syn}}) < 13.6$, comprising 90% of the sample). A fit of a linear function

$$\log(E_{\text{pk}}^{\text{IC}}) = \alpha \times \log(\nu_{\text{pk}}^{\text{syn}}) + K \quad (1)$$

(with $E_{\text{pk}}^{\text{IC}}$ in MeV and $\nu_{\text{pk}}^{\text{syn}}$ in Hz) to the BL Lac data provides $\alpha=0.366$ and $K = -1.71$. A similar fit for the FSRQs¹⁰ restricted to $\log(\nu_{\text{pk}}^{\text{syn}}) < 13.6$ yields $\alpha=0.293$ and $K = -1.03$. The trend obtained from Equation 5 in [Abdo et al. \(2010a\)](#) (derived using broad-band data from 48 bright blazars including 23 FSRQs, 23 BL Lacs and 2 BCUs) is also shown in Figure 6.

The Compton dominance is defined as the ratio between the peak νF_ν for the high- and low-frequency SED components. This redshift-independent parameter has been intensively discussed in the context of the blazar sequence (e.g., [Meyer et al. 2011](#); [Finke 2013](#); [Nalewajko & Gupta 2017](#); [Paliya et al. 2021](#)). The Compton dominance is plotted as a function of $\nu_{\text{pk}}^{\text{syn}}$ in Figure 7, together with the threshold derived from that plotted in Figure 5. The trend is very similar to that seen when the Compton dominance is assessed using the prescription of [Abdo et al. \(2010a\)](#). Fitting the BL Lac (log-log) data in Figure 7 with a linear function gives a slope of -0.46 ± 0.12 . No clear indication of an upturn around $\nu_{\text{pk}} \simeq 10^{14}$ Hz manifesting the transition between Synchrotron-Self-Compton and External-Compton as the dominant emission process ([Finke 2013](#)) is seen in Figure 7. **However, the larger scatter in Compton dominance observed for FSRQs relative to BL Lacs is likely due to this difference in main emission processes (External-Compton vs. Synchrotron-Self-Compton), in addition to different variability levels.**

6. SUMMARY

The new release (4FGL-DR3) includes about 19% more blazars than the initial 4LAC-DR1, comprising 75 FSRQs, 117 BL Lacs, 395 BCUs, and 4 radio galaxies. The large fraction of BCUs (two thirds) calls for new spectroscopic data to enable the classification. The BCU photon-index distribution suggests that the fraction of FSRQs within these BCUs is notably larger (by a factor $\simeq 2.5$) than that found in the set of classified blazars. This feature, not apparent in 4LAC-DR1, may result from a larger flaring propensity of FSRQs relative to BL Lacs in the LAT energy range, as exemplified e.g., by the very different fractions (42% vs. 6%) of variable 4FGL-DR3 sources seen in these classes. Both redshift and photon-index distributions of the new FSRQs and BL Lacs are similar to the previously detected ones. Thanks to the new data and a looser threshold regarding variability, 214 additional 4FGL-DR1 sources are now considered variable. A total of 1602 LAT blazars have a significantly curved spectrum, from which the peak position of the high-energy SED component and its corresponding flux can be estimated from the gamma-ray data alone by fitting a log normal function. These parameters combined with the position of the synchrotron peak estimated from archival data allows us to derive the Compton dominance.

REFERENCES

- ⁹ Primed quantities are evaluated in the source rest frame. For BL Lacs and BCUs without measured redshifts, values of $z=0.38$ and 0.56 , corresponding to the median measured redshifts for these two classes, have been assumed respectively.
- ¹⁰ Fitting the peak positions in the observer frame yields $\alpha=0.374$ (0.344) and $K = -1.92$ (-1.93) for BL Lacs (FSRQs).

- 313 Abdo, A. A., Ackermann, M., Ajello, M., et al. 2010b,
314 ApJS, 188, 405, (1FGL)
- 315 Abdollahi, S., Acero, F., Ackermann, M., et al. 2020, ApJS,
316 247, 33
- 317 Abdollahi, S., Acero, F., Baldini, L., et al. 2022, ApJS, 260,
318 53
- 319 Ackermann, M., Ajello, M., Allafort, A., et al. 2011, ApJ,
320 743, 171, (2LAC)
- 321 Ackermann, M., Ajello, M., Atwood, W. B., et al. 2015,
322 ApJ, 810, 14, (3LAC)
- 323 Ajello, M., Angioni, R., Axelsson, M., et al. 2020, ApJ, 892,
324 105
- 325 Atwood, W. B., Abdo, A. A., Ackermann, M., et al. 2009,
326 ApJ, 697, 1071, (LAT)
- 327 Ballet, J., Burnett, T. H., Digel, S. W., & Lott, B. 2020,
328 arXiv e-prints, arXiv:2005.11208
- 329 Britzen, S., Vermeulen, R. C., Campbell, R. M., et al. 2008,
330 A&A, 484, 119
- 331 de Menezes, R., Nemmen, R., Finke, J. D., Almeida, I., &
332 Rani, B. 2020, MNRAS, 492, 4120
- 333 Desai, A., Marchesi, S., Rajagopal, M., & Ajello, M. 2019,
334 ApJS, 241, 5
- 335 Finke, J. D. 2013, ApJ, 763, 134
- 336 Fukazawa, Y., Matake, H., Kayanoki, T., Inoue, Y., &
337 Finke, J. 2022, arXiv e-prints, arXiv:2204.14019
- 338 Goldoni, P., Pita, S., Boisson, C., et al. 2021, A&A, 650,
339 A106
- 340 Grandi, P., Capetti, A., & Baldi, R. D. 2016, MNRAS, 457,
341 2
- 342 Järvelä, E., Berton, M., Ciroi, S., et al. 2020, A&A, 636,
343 L12
- 344 Lott, B., Gasparri, D., & Ciprini, S. 2020, arXiv e-prints,
345 arXiv:2010.08406
- 346 Martí, J., Sánchez-Ayaso, E., Luque-Escamilla, P. L., et al.
347 2020, MNRAS, 492, 4291
- 348 Meyer, E. T., Fossati, G., Georganopoulos, M., & Lister,
349 M. L. 2011, ApJ, 740, 98
- 350 Nalewajko, K., & Gupta, M. 2017, A&A, 606, A44
- 351 NASA/IPAC Extragalactic Database (NED). 2019,
352 NASA/IPAC Extragalactic Database (NED), IPAC,
353 doi:10.26132/NED1
- 354 Paliya, V. S. 2021, The Astrophysical Journal Letters, 918,
355 L39
- 356 Paliya, V. S., Domínguez, A., Ajello, M., Olmo-García, A.,
357 & Hartmann, D. 2021, ApJS, 253, 46
- 358 Paliya, V. S., Domínguez, A., Cabello, C., et al. 2020a,
359 ApJL, 903, L8
- 360 Paliya, V. S., Pérez, E., García-Benito, R., et al. 2020b,
361 ApJ, 892, 133
- 362 Peña-Herazo, H. A., Marchesini, E. J., Álvarez Crespo, N.,
363 et al. 2017, Ap&SS, 362, 228
- 364 Peña-Herazo, H. A., Massaro, F., Chavushyan, V., et al.
365 2019, Ap&SS, 364, 85
- 366 Peña-Herazo, H. A., Amaya-Almazán, R. A., Massaro, F.,
367 et al. 2020, A&A, 643, A103
- 368 Peña-Herazo, H. A., Massaro, F., Gu, M., et al. 2021a, AJ,
369 161, 196
- 370 —. 2021b, AJ, 162, 76
- 371 Peña-Herazo, H. A., Paggi, A., García-Pérez, A., et al.
372 2021c, AJ, 162, 177
- 373 Rajagopal, M., Marchesi, S., Kaur, A., et al. 2021, ApJS,
374 254, 26
- 375 Saldana-Lopez, A., Domínguez, A., Pérez-González, P. G.,
376 et al. 2021, MNRAS, 507, 5144
- 377 van Velzen, S., Falcke, H., Schellart, P., Nierstenhöfer, N.,
378 & Kampert, K.-H. 2012, A&A, 544, A18
- 379 Wrobel, J. M., & Heeschen, D. S. 1984, ApJ, 287, 41

7. ACKNOWLEDGMENTS

The *Fermi* LAT Collaboration acknowledges generous ongoing support from a number of agencies and institutes that have supported both the development and the operation of the LAT as well as scientific data analysis. These include the National Aeronautics and Space Administration and the Department of Energy in the United States, the Commissariat à l’Energie Atomique and the Centre National de la Recherche Scientifique / Institut National de Physique Nucléaire et de Physique des Particules in France, the Agenzia Spaziale Italiana and the Istituto Nazionale di Fisica Nucleare in Italy under ASI-INFN Agreements No. 2021-43-HH.0, the Ministry of Education, Culture, Sports, Science and Technology (MEXT), High Energy Accelerator Research Organization (KEK) and Japan Aerospace Exploration Agency (JAXA) in Japan, and the K. A. Wallenberg Foundation, the Swedish Research Council and the Swedish National Space Board in Sweden. Additional support for science analysis during the operations phase is gratefully acknowledged from the Istituto Nazionale di Astrofisica in Italy and the Centre National d’Études Spatiales in France. This work performed in part under DOE Contract DE-AC02-76SF00515.

This research has made use of the [NASA/IPAC Extragalactic Database \(NED\)](#) (2019) which is operated by the Jet Propulsion Laboratory, California Institute of Technology, under contract with the National Aeronautics and Space Administration, and of archival data, software and online services provided by the ASI Space Science Data Center (SSDC) operated by the Italian Space Agency.

APPENDIX

A. DESCRIPTION OF THE FITS VERSION OF THE 4LAC-DR3 CATALOG

Table A1. 4LAC-DR3 FITS Format

Column	Format	Unit	Description
Source_Name	18A	...	Source name 4FGL JHHMM.m+DDMMa ^a
DataRelease	I		1 for 4FGL, 2 for new in DR2, 3 for new or changed in DR
RAJ2000	E	deg	Right Ascension
DEJ2000	E	deg	Declination
GLON	E	deg	Galactic Longitude
GLAT	E	deg	Galactic Latitude
Signif_Avg	E	...	Source significance in σ units over the 50 MeV to 1 TeV band
Flux1000	E	cm ⁻² s ⁻¹	Integral photon flux from 1 to 100 GeV
Unc_Flux1000	E	cm ⁻² s ⁻¹	1 σ error on integral photon flux from 1 to 100 GeV
Energy_Flux100	E	erg cm ⁻² s ⁻¹	Energy flux from 100 MeV to 100 GeV obtained by spectral fitting
Unc_Energy_Flux100	E	erg cm ⁻² s ⁻¹	1 σ error on energy flux from 100 MeV to 100 GeV
SpectrumType	17A	...	Spectral type in the global model (PowerLaw, LogParabola, PLSuperExpCutoff)
PL_Index	E	...	Photon index when fitting with PowerLaw
Unc_PL_Index	E	...	1 σ error on PL_Index
Pivot_Energy	E	MeV	Pivot Energy
LP_Index	E	...	Photon index at Pivot_Energy (α) when fitting with LogParabola
Unc_LP_Index	E	...	1 σ error on LP_Index
LP_beta	E	...	Curvature parameter (β) when fitting with LogParabola
Unc_LP_beta	E	...	1 σ error on LP_beta
Flags	I	...	Analysis flags
CLASS	6A	...	Class designation for associated source
ASSOC1	30A	...	Name of identified or likely associated source
ASSOC_PROB_BAY	E	...	Probability of association according to the Bayesian method
ASSOC_PROB_LR	E	...	Probability of association according to the Likelihood Ratio method
Counterpart_Catalog	10A		Counterpart catalog driving the association
RA_Counterpart	D	deg	Right Ascension of the counterpart ASSOC1
DEC_Counterpart	D	deg	Declination of the counterpart ASSOC1
Unc_Counterpart	E	deg	95% precision of the counterpart localization
VLBI_Counterpart	14A	...	Name of the VLBI counterpart
Redshift	E	...	Redshift
SED_class	6A	...	SED-based class
HE_EPeak	E	MeV	Energy in the observer frame of the high-energy SED peak
Unc_HE_EPeak	E	MeV	1 σ error on energy of the high-energy SED peak
HE_nuFnuPeak	E	erg cm ⁻² s ⁻¹	$\nu F\nu$ at high-energy-peak frequency
Unc_HE_nuFnuPeak	E	erg cm ⁻² s ⁻¹	1 σ error on spectral energy distribution at high-energy-peak frequency
nu_syn	E	Hz	synchrotron-peak frequency in the observer frame
nuFnu_syn	E	erg cm ⁻² s ⁻¹	$\nu F\nu$ at synchrotron-peak frequency
Variability_Index	E	...	Variability index
Frac_Variability	E	...	Fractional variability
Unc_Frac_Variability	E	...	1 σ error on fractional variability
Highest_energy	E	GeV	energy (if greater than 10 GeV) of the highest-energy ULTRACLEANVETO photon with association probability $P > 0.95$